International Journal of Heat and Mass Transfer 52 (2009) 3101–3108

Contents lists available at ScienceDirect

International Journal of Heat and Mass Transfer

journal homepage: www.elsevier.com/locate/ijhmt

Asymptotic behaviors of heat transfer in porous passages with axial conduction

W.J. Minkowycz [a], A. Haji-Sheikh [b,*]

[a] Department of Mechanical and Industrial Engineering, University of Illinois at Chicago, Chicago, IL 60607-7022, USA
[b] Department of Mechanical and Aerospace Engineering, The University of Texas at Arlington, Arlington, TX 76019-0023, USA

ARTICLE INFO

Article history:
Received 12 November 2008
Received in revised form 20 January 2009
Accepted 20 January 2009
Available online 5 April 2009

Keywords:
Heat transfer
Convection
Axial conduction
Duct flow
Thermal entrance
Parallel-plate ducts

ABSTRACT

As reported in the literature, a sufficiently small Peclet number requires the inclusion of axial conduction within a fluid flowing in a duct. In fluid saturated porous ducts, this phenomenon greatly increases the heat transfer rate within the thermal entrance region. Axial conduction effects near the thermal entrance regions in parallel-plate ducts and in circular ducts are emphasized in this study. Having metallic foams as porous materials can cause the effective thermal conductivity to increase and this decreases the Peclet number. Here, a simple solution is being used for determination wall heat flux near the thermal entrance location and the result leads to a relatively simple correlation for determination of the bulk temperature.

1. Introduction

For passages filled with relatively high thermal conductivity porous materials, the contribution of axial conduction becomes significant [1]. The inclusion of the axial conduction within the exact solutions of temperature fields in parallel-plate channels and circular ducts lead to modified Graetz type solutions, as reported in [1]. Also, for flow through a porous medium Nield et al. numerically studied the contribution of axial conduction in flow between two parallel plates in [2] and circular porous passages in [3]. These reported numerical Nusselt number values indicate significant variations depending on the size of the Peclet number.

The studies of heat transfer in the absence of axial conduction are available in the literature [4–12]. Because, the placement of porous materials in flow passages can enhance the heat transfer rate, there is a recent interest in using this concept for electronic cooling applications [12]. As stated earlier, the axial conduction strongly affects the transport of thermal energy to fluid flowing through porous passages, near the entrance region. Accordingly, the understanding of the wall heat flux phenomena near the thermal entrance region is emphasized in this presentation.

The reported study in [13] uses a closed form analytical solution to show that conduction dominates near the location of an abrupt temperature change. This study suggests that the effect of the Darcy number diminishes near the thermal entrance region as the Peclet number becomes small. Because, as shown in [13], the fluid velocity has a relatively small effect on heat transfer coefficient near the location where there is an abrupt temperature change. The verification of the validity of this concept is one of the topics in this presentation. To accomplish this task, the data reported in [1] are augmented and being used in this study. Therefore, this work becomes an extension of the earlier study reported in [1]. However, for completeness of this presentation, a summary of the analyses in [1] is included in the following sections.

2. Velocity fields

Consideration is given to a steady and hydrodynamically fully developed flow between two impermeable parallel plates and for flow through a circular passage with an impermeable wall, as shown in Fig. 1. Although the extended Graetz-type solution details are in [1] and [5], a summary is presented here.

The solution of Brinkman momentum equation provides the velocity field between two parallel plates $2H$ apart. In dimensionless space, when $\bar{y} = y/H$ and $\bar{u} = \mu u/(\Phi H^2)$, it is

$$\bar{u} = \mathrm{Da}\left[1 - \frac{\cosh(\omega\bar{y})}{\cosh(\omega)}\right] \tag{1}$$

where $\Phi = -\partial p/\partial x, \omega = (M\,\mathrm{Da})^{-1/2}, M = \mu_e/\mu, \mathrm{Da} = K/H^2$, μ is the fluid viscosity, μ_e the effective viscosity, and K is the permeability. Using the definition of the average velocity,

* Corresponding author. Tel.: +1 817 272 2010; fax: +1 817 272 2952.
E-mail address: haji@uta.edu (A. Haji-Sheikh).

0017-9310/$ - see front matter © 2009 Elsevier Ltd. All rights reserved.
doi:10.1016/j.ijheatmasstransfer.2009.01.032

Nomenclature

A	area, m^2
B_m	coefficient
Br	Brinkman number, $\mu U^2/[\mathrm{Da}k_e(T_1-T_2)]$
C	duct contour, m
c_n	coefficients
c_p	specific heat, J/kg K
Da	Darcy number, K/H^2 or K/r_0^2
D_h	hydraulic diameter, m
d_n	coefficients
F	pressure coefficient
f	Moody friction factor
h	heat transfer coefficient W/m^2 K
$\bar{h}$	average heat transfer coefficient W/m^2 K
i, j	indices
K	permeability, m^2
k_e	effective thermal conductivity
L_c	characteristic length, H or r_0, m
M	μ_e/μ
Nu	Nusselt numbed hL_c/k
Nu_D	Nusselt numbed hD_e/k
m,n	indices
p	pressure, Pa
Pe	Peclet number, $\rho c_p L_c U/k_e$
Pr	Prandtl number, $\mu c_p/k_e$
r	radial coordinate
r_0	pipe radius, m
S	volumetric heat source, W/m^3
T	temperature, K
T_i	temperature in region 1 or 2
T_w	wall temperature, K
u	velocity, m/s
$\bar{u}$	$\bar{u} = \mu u/(\Phi L_c^2)$
U	average velocity, m/s
$\bar{U}$	average value of $\bar{u}$
x	axial coordinate, m
$\bar{x}$	$x/(\mathrm{Pe}H)$ or $\bar{x} = x/(\mathrm{Per}_0)$
y	coordinates, m
$\bar{y}$	y/a

Greek

β	coefficients
Φ	$-\partial p/\partial x$
λ_m	eigenvalues
θ_i	$(T - T_i)/(T_1-T_2)$, $i = 1$ or 2
μ	fluid viscosity, N s/m^2
μ_e	effective viscosity, N s/m^2
ψ_m	eigenfunctions
ρ	density, kg/m^3
η	y/H or r/r_0
ω	parameter, $1/\sqrt{M\mathrm{Da}}$

Subscripts

L	large
S	small
w	wall

$$\bar{U} = \int_0^1 \bar{u}d\bar{y} = \mathrm{Da}\left[1 - \frac{\tanh(\omega)}{\omega}\right], \tag{2}$$

the dimensionless velocity takes the form

$$\frac{u}{U} = \frac{\bar{u}}{\bar{U}} = \frac{\omega}{\omega - \tanh(\omega)}\left[1 - \frac{\cosh(\omega\bar{y})}{\cosh(\omega)}\right] \tag{3}$$

for inclusion in the energy equation.

Similarly, the velocity field within a fluid saturated circular passage with radius r_o, as given in [1,5] is

$$\bar{u} = \mathrm{Da}\left[1 - \frac{I_0(\omega\bar{r})}{I_0(\omega)}\right] \tag{4}$$

where $\bar{r} = r/r_0, \bar{u} = \mu u/(\Phi r_0^2)$, $\mathrm{Da} = K/r_0^2$, and $\omega = (M\,\mathrm{Da})^{-1/2}$. Also, by definition, the mean velocity is

$$U = \frac{2}{r_0^2}\int_0^{r_0} urdr \tag{5}$$

and the dimensionless velocity profile take the following form

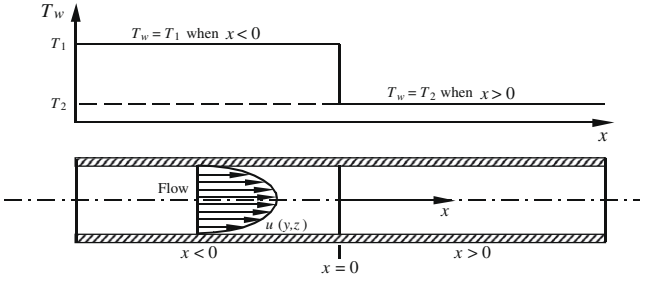

Fig. 1. Schematic of a duct with prescribed surface temperatures.

$$\frac{u}{U} = \frac{\bar{u}}{\bar{U}} = \frac{\omega I_0(\omega)}{\omega I_0(\omega) - 2I_1(\omega)}\left[1 - \frac{I_0(\omega\bar{r})}{I_0(\omega)}\right]. \tag{6}$$

3. Temperature solutions

The energy equation assuming local thermal equilibrium, as reported in [1] for these two channels are

$$u\frac{\partial T}{\partial x} = \frac{k_e}{\rho c_p}\left(\frac{\partial^2 T}{\partial x^2} + \frac{\partial^2 T}{\partial y^2}\right) \tag{7}$$

for parallel-plate ducts and

$$u\frac{\partial T}{\partial x} = \frac{k_e}{\rho c_p}\left(\frac{\partial^2 T}{\partial r^2} + \frac{1}{r}\frac{\partial T}{\partial r} + \frac{\partial^2 T}{\partial x^2}\right) \tag{8}$$

for circular ducts. In the dimensionless space the axial coordinate is $\bar{x} = x/(\mathrm{Pe}H)$ where $\mathrm{Pe} = UH/\alpha$ for parallel-plate ducts while for circular ducts $\bar{x} = x/(\mathrm{Pe}\,r_0)$ where $\mathrm{Pe} = \rho c_p r_0 U/k_e$. In this formulation, T_1 is the wall temperature when $x < 0$ and T_2 is the wall temperature when $x > 0$. Accordingly, the appropriate dimensionless temperatures forms are $\theta_1 = (T - T_1)/(T_1 - T_2)$ when $x < 0$ and $\theta_2 = (T - T_2)/(T_1 - T_2)$ when $x > 0$. Then, in the dimensionless space, Eqs. (7) and (8) are being combined and they take the form

$$\frac{1}{\eta^e}\frac{\partial}{\partial\eta}\left(\eta^e\frac{\partial\theta_i}{\partial\eta}\right) = \frac{u}{U}\frac{\partial\theta_i}{\partial\bar{x}} - \frac{1}{\mathrm{Pe}^2}\frac{\partial^2\theta_i}{\partial\bar{x}^2}. \tag{9}$$

In this equation, for parallel-plate ducts, $e = 0$ and parameter η stands for the dimensionless Cartesian coordinate y/H while for circular ducts $e = 1$ and parameter η stands for the dimensionless radial coordinate r/r_0. The reduced forms of temperature solutions of Eq. (9) for θ_1 and θ_2, as given in [1], are

$$\theta_1 = \sum_{m=1}^{\infty} A_m \psi_m(\eta) e^{\lambda_m^2 \bar{x}} \quad \text{when } x < 0 \tag{10}$$

and

$$\theta_2 = \sum_{m=1}^{\infty} B_m \psi_m(\eta) e^{-\lambda_m^2 \bar{x}} \quad \text{when } x > 0 \tag{11}$$

where the eigenvalues λ_m are real but different for θ_1 and θ_2 solutions while

$$\psi_m(\eta) = \sum_{n=0}^{\infty} c_n \eta^n. \tag{12}$$

The method of determination of λ_m and coefficients c_n are in [1]. Once the eigenvalues are known, the orthogonality condition

$$\int_0^1 \left[\frac{\lambda_m^2 + \lambda_n^2}{\mathrm{Pe}^2} - \frac{u(\eta)}{U}\right] \psi_n(\eta)\psi_m(\eta) \times \eta^e d\eta = \begin{cases} 0 & \text{when } n \neq m \\ N_m & \text{when } n = m \end{cases} \tag{13}$$

provides the coefficients A_m and B_m as

$$A_m = \frac{2}{\lambda_m} \frac{1}{[d\psi_m(\eta)/d\lambda_m]_{\eta=1}} \tag{14a}$$

and

$$B_m = -\frac{2}{\lambda_m} \frac{1}{[d\psi_m(\eta)/d\lambda_m]_{\eta=1}}. \tag{14b}$$

Numerical values of the Nusselt number and the bulk temperature for different Pe and *M*Da parameters from [1] are being used to evaluate the application of findings reported in [13] to heat transfer in porous passage. The numerical data are acquired for the Nusselt number [1] from the equation

$$\mathrm{Nu}_D = hD_h/k_e = -\frac{2(2-e)}{\theta_b} \sum_{m=1}^{\infty} B_m \left.\frac{d\psi_m(\eta)}{d\eta}\right|_{\eta=1} e^{-\lambda_m^2 \bar{x}} \tag{15}$$

and for the bulk temperature from the relation

$$\theta_b = \frac{T_b - T_2}{T_1 - T_2} = (1+e) \sum_{m=1}^{\infty} B_m e^{-\lambda_m^2} \int_0^1 \left(\frac{u}{U}\right) \psi_m(\eta) \eta^e d\eta \tag{16}$$

where $e = 0$ for Cartesian coordinates and $e = 1$ for cylindrical coordinates.

The exact analysis can provide accurate solutions for the Nusselt number when x is relatively large. At small values of $\bar{x}$, the number of eigenvalues must be substantially increased. The study presented in [13] leads to a methodology that would provide a remedy for this situation.

4. Solutions at small-*x* values

The study in [13] concerns with a fluid in a semi-infinite region flowing at a constant velocity over a flat plate. The result leads to a closed-form solution for determination of heat transfer using the slug flow condition. The heat transfer coefficient defined in [13] as $h_0 = q_w/(T_w - T_i)$ is being used here. Therefore, the dimensionless quantity representing this heat transfer coefficient is the Nusselt number $\mathrm{Nu}_0 = h_0 H/k_e$ for parallel-plate ducts and $\mathrm{Nu}_0 = h_0 r_0/k_e$ for circular ducts. Since the Stanton number is $\mathrm{St} = \mathrm{Nu}_0/\mathrm{Pe}$, then Eq. (23b) in [13] leads to the relation

$$\mathrm{Nu}_{0,S} = \frac{\mathrm{Pe}}{2\pi} \exp[\mathrm{Pe}(x/L_c)/2]\{K_0[\mathrm{Pe}(x/L_c)/2] + K_1[\mathrm{Pe}(x/L_c)/2]\} \tag{17a}$$

where $K_0[\mathrm{Pe}(x/L_c)/2]$ and $K_1[\mathrm{Pe}(x/L_c)/2]$ are the modified Bessel functions. As an accurate estimation, Eq. (17a), for a range of $Pe(x/L_c) < 2$, can be written as

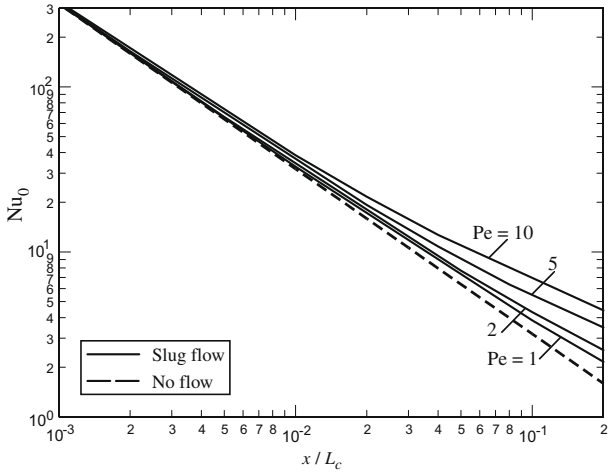

Fig. 2. The Nusselt number for slug flow over a flat plate, for a semi-infinite medium.

$$\mathrm{Nu}_{0,S} \cong \frac{\exp[\mathrm{Pe}(x/L_c)/2]}{2\pi(x/L_c)} \Big\{2 - \mathrm{Pe}(x/L_c)\Big[0.5772[1 + \mathrm{Pe}^2(x/L_c)^2/8] + [1 - \mathrm{Pe}(x/L_c)4 + \mathrm{Pe}^2(x/L_c)^2/8]\ln(x\mathrm{Pe}/4L_c)\Big]\Big\}. \tag{17b}$$

The solid lines in Fig. 2 show the values of Nu_0 for Pe = 1, 2, 5, 10, computed using Eq. (17a). As x becomes small, the solid lines approach the dash line that represents the values of $\mathrm{Nu}_0 = 1/[\pi(x/L_c)]$, for pure conduction when the fluid velocity is equal to zero. Also, it can be shown mathematically that Eq. (17a) or Eq. (17b) would approach asymptotically to $\mathrm{Nu}_0 = 1/[\pi(x/L_c)]$ as $\mathrm{Pe} \to 0$.

The dot-dash lines with symbols plotted in Fig. 3(a) are taken from the solutions in [1] for Pe = 1. The dot-dash lines describe a broad range of *M*Da values 10^{-5}, 10^{-3}, and 1 and they are identified by designated symbols. The dash line and the solid line as they appear in Fig. 3(a) are imported from Fig. 2. They clearly show that for a small Peclet numbers, the discrete symbols are located between the dash line and the solid line while the *M*Da effect is being very small. Therefore, the dash line can provide a limiting condition as x becomes very small. Fig. 3(a) clearly shows a unique feature of this small-x solution when Pe is small. As can be seen, the effect of the *M*Da values on the Nusselt number Nu_0 diminishes at relatively small Pe values. To further elaborate on this issue, Fig. 3(b) contains discrete data imported also from [1] for Pe = 2 and prepared in a similar manner as described for Fig. 3(a). Again, the symbols are clearly located between the solid line and the dash line. However, the influence of *M*Da values on Nu_0 is slightly larger. This process is repeated for Pe = 5 and 10 and discrete data are plotted in Fig. 3(c and d), respectively. The results show similar behaviors while the influence of the *M*Da values on Nu_0 is increasing as Pe increases. It is remarkable that the line for slug flow clearly passes through the symbols for *M*Da = 10^{-5} and the symbols for *M*Da = 1 arrive toward the line for no flow passes, as x decreases.

The application of the asymptotic solution to circular passages can show the curvature effect. The discrete symbols in Fig. 4(a–d) are also taken from the series solution. Fig. 4(a) shows that the data at small x values behave similar to those in Fig. 3(a). Therefore, the dash line or the solid line can provide a reasonable asymptotic solution. Also, these figures show that the effect of *M*Da values on Nu_0 become small as Pe reduces. The effect of curvature on the Nu_0 values is clearly detectable by comparing the "×" symbols in Fig. 4(d) with those in Fig. 3(d). In Fig. 4(d), the "×" symbols are located along the solid line for $x/r_0 < 0.02$. In Fig. 3(d), these symbols remain along the solid line for a relatively long distance while, in Fig. 4(d), the "×" symbols begin to depart from the solid line near $x/r_0 \sim 0.02$.

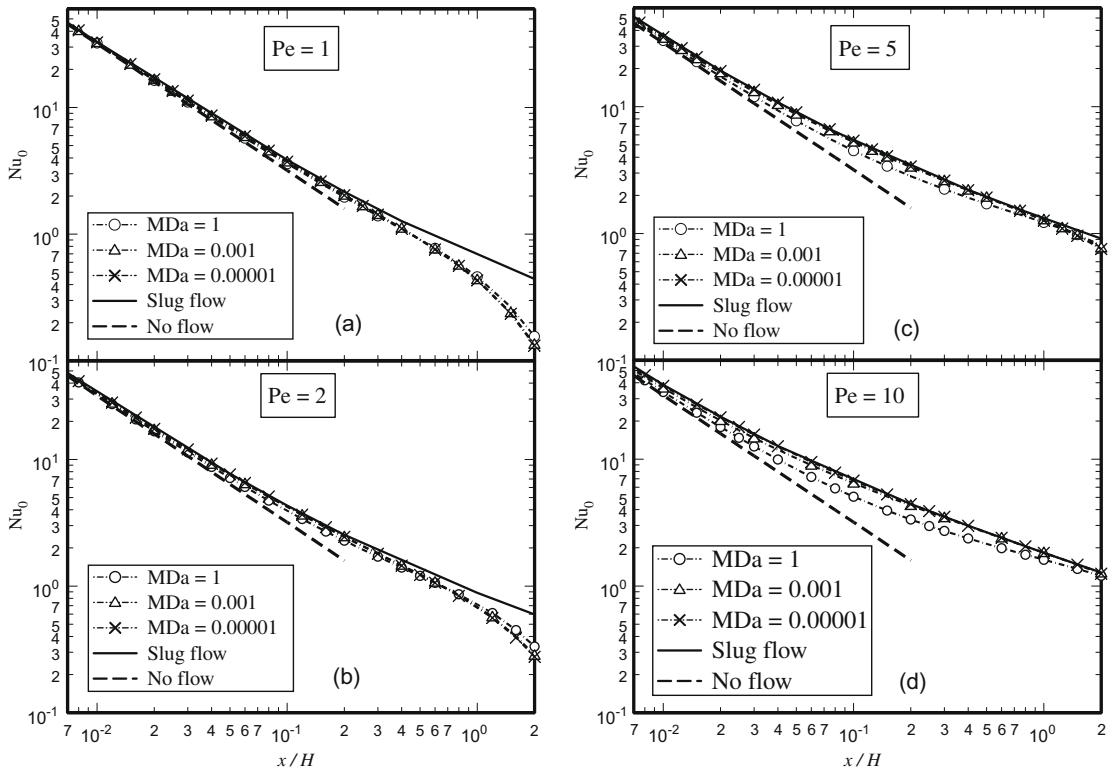

Fig. 3. Local Nusselt number for parallel plate ducts (a) when Pe = 1, (b) when Pe = 2, (c) when Pe = 5, and (d) when Pe = 10.

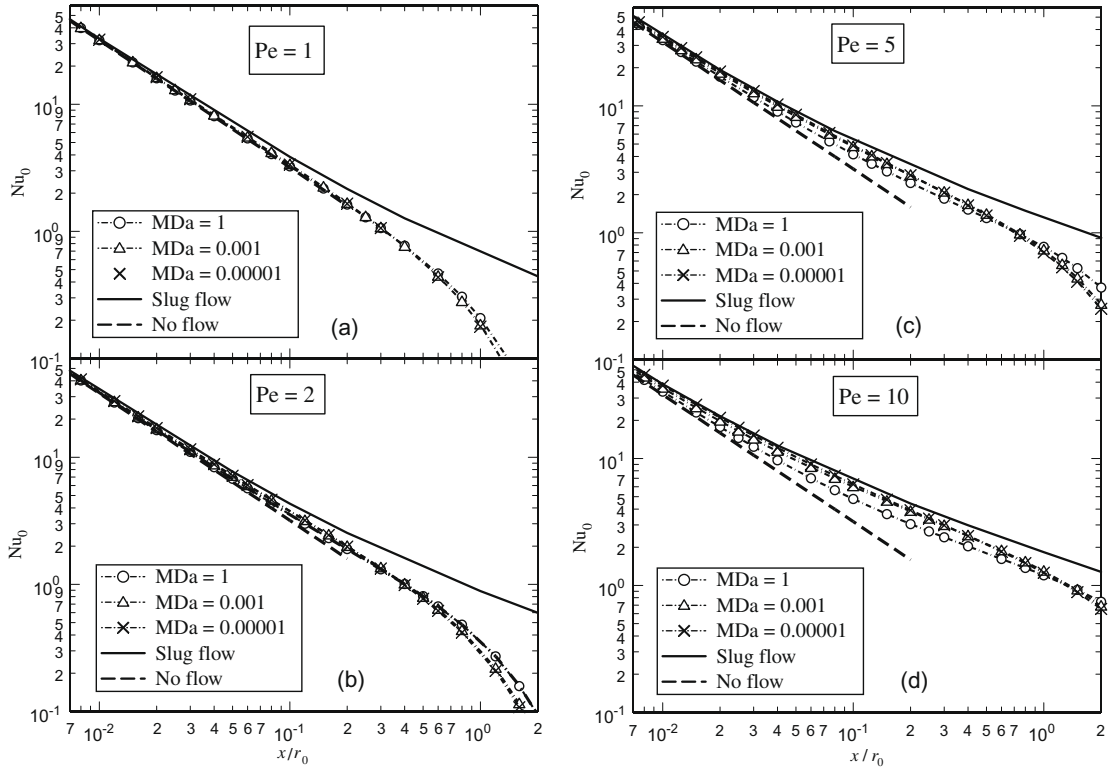

Fig. 4. Local Nusselt number for circular ducts (a) when Pe = 1, (b) when Pe = 2, (c) when Pe = 5, and (d) when Pe = 10.

Table 1
Parameters for determination of asymptotic values for parallel-plate ducts.

MDa	Pe	λ_1^2	C_1^+	D_1^+	$\theta_b(0)$	Nu(∞)
1	0.5	0.6400	1.145	0.5748	0.5893	1.992
	1	1.0511	1.275	0.6500	0.669	1.961
	2	1.4799	1.461	0.7568	0.784	1.930
	3	1.6442	1.564	0.8159	0.849	1.917
	5	1.8009	1.653	0.8668	0.910	1.908
	7	1.847	1.686	0.8856	0.937	1.904
	10	1.8736	1.706	0.8967	0.956	1.902
10^{-2}	0.5	0.6597	1.161	0.5128	0.576	2.265
	1	1.1139	1.309	0.5799	0.646	2.258
	2	1.6343	1.537	0.6832	0.755	2.250
	3	1.8829	1.678	0.7471	0.825	2.246
	5	2.0830	1.813	0.8083	0.895	2.243
	7	2.1546	1.867	0.8326	0.927	2.242
	10	2.1968	1.900	0.8478	0.951	2.241
10^{-3}	0.5	0.6669	1.161	0.4849	0.571	2.394
	1	1.1373	1.309	0.5472	0.636	2.393
	2	1.6946	1.544	0.6457	0.741	2.392
	3	1.9717	1.696	0.7093	0.810	2.391
	5	2.2022	1.847	0.7725	0.884	2.391
	7	2.2867	1.909	0.7986	0.919	2.390
	10	2.3372	1.948	0.8151	0.945	2.390
10^{-5}	0.5	0.6699	1.158	0.4707	0.567	2.460
	1	1.1473	1.304	0.5302	0.630	2.460
	2	1.7213	1.538	0.6258	0.732	2.460
	3	2.0114	1.692	0.6878	0.801	2.460
	5	2.2566	1.847	0.7511	0.875	2.460
	7	2.3474	1.913	0.7777	0.911	2.460
	10	2.4021	1.954	0.7945	0.938	2.460

Table 2
Parameters for determination of asymptotic values for circular ducts.

MDa	Pe	λ_1^2	C_1^+	D_1^+	$\theta_b(0)$	Nu(∞)
1	0.5	1.0238	1.076	0.5301	0.564	2.029
	1	1.7492	1.149	0.5811	0.624	1.978
	2	2.6123	1.271	0.6622	0.720	1.919
	3	3.0427	1.351	0.7148	0.786	1.890
	5	3.4014	1.432	0.7672	0.859	1.866
	7	3.5332	1.466	0.7889	0.895	1.858
	10	3.6119	1.487	0.8026	0.925	1.853
10^{-2}	0.5	1.0610	1.106	0.4496	0.551	2.460
	1	1.8759	1.207	0.4937	0.600	2.445
	2	2.9672	1.382	0.5698	0.685	2.426
	3	3.5985	1.513	0.6265	0.750	2.415
	5	4.2044	1.668	0.6935	0.832	2.405
	7	4.4546	1.742	0.7257	0.876	2.401
	10	4.6136	1.794	0.7480	0.913	2.398
10^{-3}	0.5	1.0766	1.108	0.4066	0.544	2.725
	1	1.9304	1.212	0.4451	0.587	2.722
	2	3.1295	1.397	0.5136	0.665	2.719
	3	3.8676	1.542	0.5674	0.727	2.718
	5	4.6245	1.727	0.6358	0.811	2.716
	7	4.9567	1.823	0.6714	0.859	2.715
	10	5.1759	1.892	0.6972	0.900	2.714
10^{-5}	0.5	1.0832	1.104	0.3842	0.541	2.873
	1	1.9537	1.205	0.4193	0.580	2.873
	2	3.2011	1.386	0.4823	0.652	2.873
	3	3.9893	1.532	0.5330	0.711	2.873
	5	4.8223	1.723	0.5995	0.794	2.873
	7	5.1984	1.826	0.6354	0.843	2.873
	10	5.4514	1.902	0.6620	0.886	2.873

Now, it is possible to present the asymptotic behaviors of the Nusselt number values. At small values of x, the effect of Darcy numbers disappears and the asymptotic values of the Nusselt number is the same as those in [14,15]. At large values of x, one-term solutions for the Nusselt number and bulk temperature are

$$\mathrm{Nu}_0 = -B_1 \frac{d\psi_1(\eta)}{d\eta}\bigg|_{\eta=1} e^{-\lambda_1^2 \bar{x}} = C_1^+ e^{-\lambda_1^2 \bar{x}} \tag{18}$$

$$\theta_b = (1+e)B_1 e^{-\lambda_1^2} \int_0^1 \left(\frac{u}{U}\right)\psi_1(\eta)\eta^e d\eta = D_1^+ e^{-\lambda_1^2}. \tag{19}$$

The coefficients λ_1^2, C_1^+, and D_1^+, when x is positive, are in Tables 1 and 2, for selected MDa and Pe parameters. The error for each entry is mainly due to the truncation error within the last digit. These relations show that the large-x asymptotic solution for the Nusselt number reduces to

$$\frac{hL_c}{k} = \left(\frac{\mathrm{Nu}_0}{\theta_b}\right) = \left(\frac{C_1^+}{D_1^+}\right) \tag{20}$$

and it becomes the thermally fully-developed value.

Knowledge of the bulk temperature in these passages is often needed in the design of heat transfer devices. As shown in [14] for parallel-plate ducts and in [15] for circular ducts, the bulk temperature can be estimated if certain variables are available. For free flow through channels [16], a single correlation provided the bulk temperature values with reasonable accuracy; that is [14,15],

$$\theta_b(x) = \left[\frac{(x/L_c)D_1^+ + \beta\theta_b(0)}{(x/L_c)+\beta}\right]\exp(-\lambda_1^2\bar{x}) \tag{21a}$$

where β = 0.25 and L_c is the characteristic length. This relation can be modified in order to include the effect of MDa values. Clearly, the values of $\theta_b(0)$, λ_1^2 and D_1^+ are in Tables 1 and 2 for a range of Pe and MDa values. Using a modified form of parameter β, this equation equally applies to these two passages, when filled with porous materials. Accordingly, the parameter β for these porous passages depends on the Darcy and Peclet numbers and it can be estimated from the relation

$$\beta \cong 0.1 + 0.15\left(\frac{1}{1+0.15\omega/\mathrm{Pe}^{1.7}}\right) \tag{21b}$$

where $\omega = 1/\sqrt{M\mathrm{Da}}$. It is to be noted that for free flow in these passages ω = 0 and that makes β = 0.25. Figs. 5–10(b) include the contribution of these asymptotic solutions that is valid over the entire

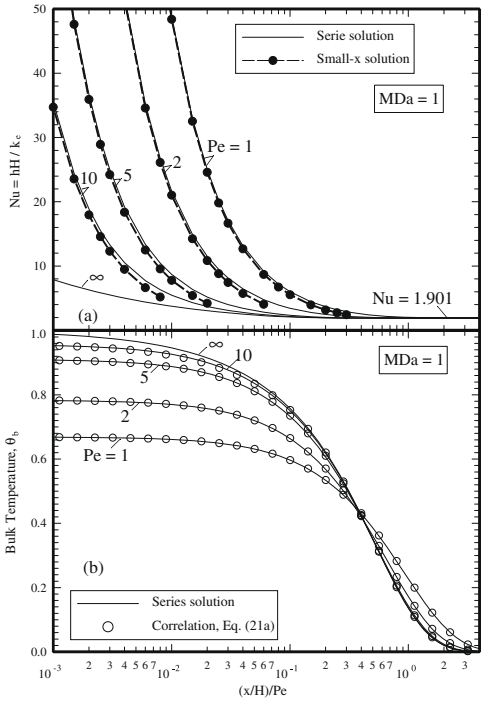

Fig. 5. The parallel plate ducts asymptotic values (a) for the Nusselt number Nu = hH/k_e and (b) for the bulk temperature as a function of (x/H)/Pe when MDa = 1.

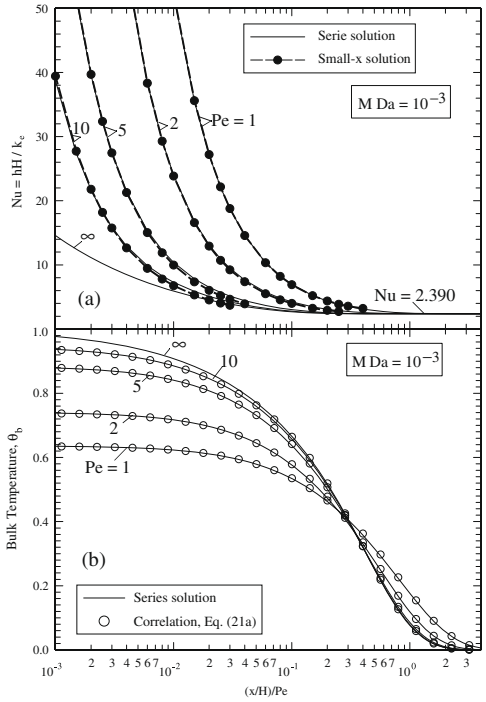

Fig. 6. The parallel plate ducts asymptotic values (a) for the Nusselt number Nu = hH/k_e and (b) for the bulk temperature as a function of $(x/H)/\mathrm{Pe}$ when $M\mathrm{Da} = 10^{-3}$.

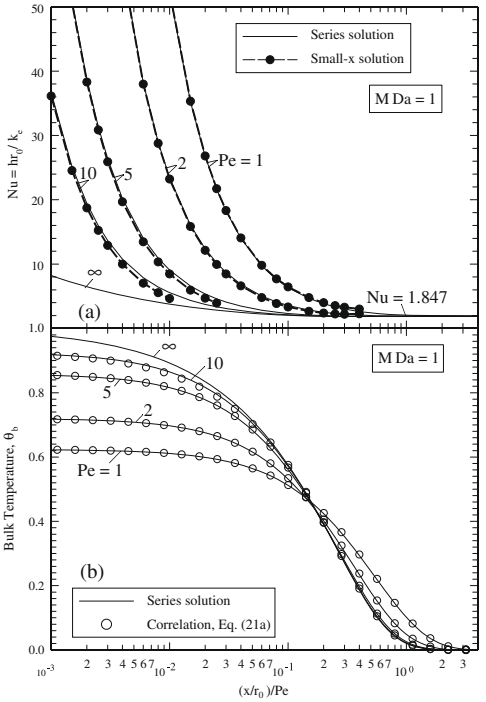

Fig. 8. The circular ducts asymptotic values (a) for the Nusselt number Nu = hH/k_e and (b) for the bulk temperature as a function of $(x/r_0)/\mathrm{Pe}$ when $M\mathrm{Da} = 1$.

range of listed parameters. The symbols in Figs. 5–7(b) show the values of bulk temperature from Eqs. (21a). These figures also include the bulk temperature values imported from [1], for parallel plate channels. The plotted symbols taken from this correlation agree well with the solid lines from [1]. This comparison process is repeated for circular ducts and the results are presented in Figs. 8–10(b). These figures show reasonably good agreements between the bulk temperature values from Eq. (21a) and computed values using the series solution, for these two ducts.

An examination of Figs. 3 and 4(a–d) shows that for each Pe, the Nu_0 values at different $M\mathrm{Da}$ parameters are located within a narrow band between the solid line and the dash line. Therefore, it is possible to use Eq. (17a) in order to estimate the values of $\mathrm{Nu}_{0,S}$ at small values of the axial coordinate. To accomplish this

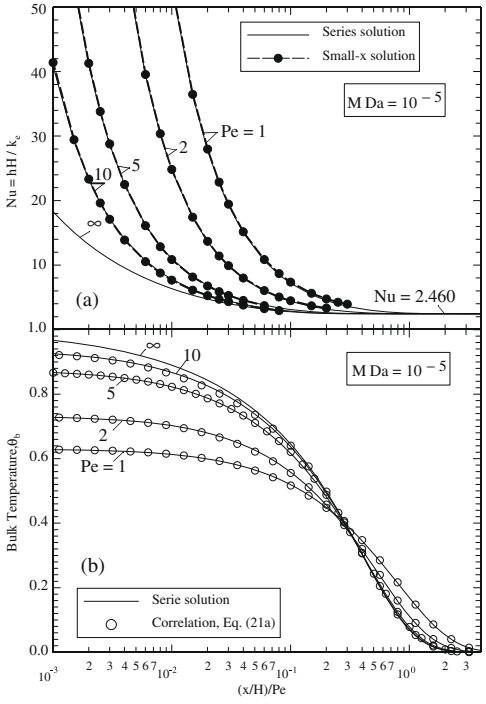

Fig. 7. The parallel plate ducts asymptotic values (a) for the Nusselt number Nu = hH/k_e and (b) for the bulk temperature as a function of $(x/H)/\mathrm{Pe}$ when $M\mathrm{Da} = 10^{-5}$.

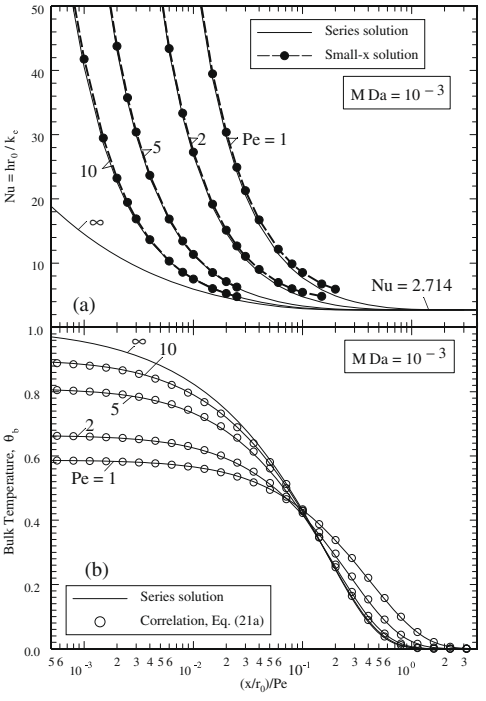

Fig. 9. The circular ducts asymptotic values (a) for the Nusselt number Nu = hH/k_e and (b) for the bulk temperature as a function of $(x/r_0)/\mathrm{Pe}$ when $M\mathrm{Da} = 10^{-3}$.

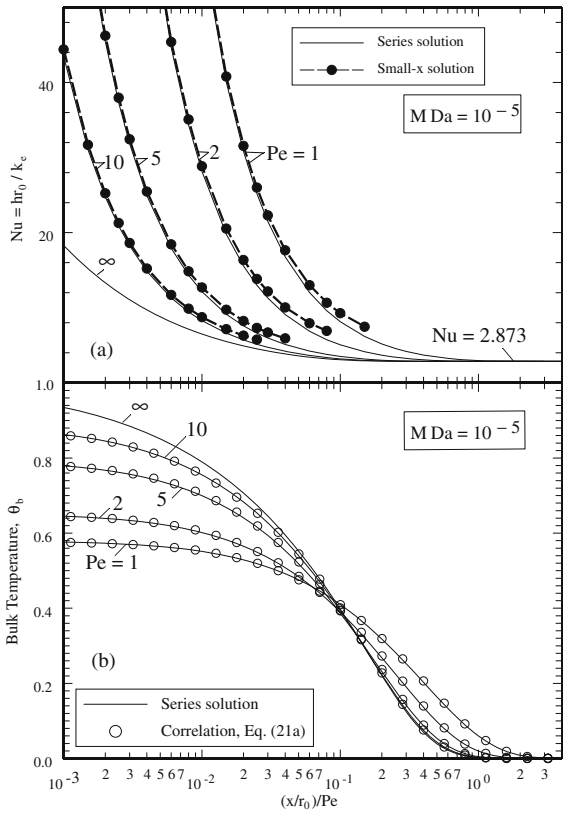

Fig. 10. The circular ducts asymptotic values (a) for the Nusselt number Nu = hH/k_e and (b) for the bulk temperature as a function of (x/r_0)/Pe when MDa = 10^{-5}.

task, as an approximation, the parameter Pe in Eq. (17a) is to be replaced by

$$\mathrm{Pe}^{*} = \mathrm{Pe}\left[\frac{1}{1+7(M\mathrm{Da})^{0.4}}\right]. \tag{22}$$

Using this transformation, the Eq. (17a) can provide reasonably accurate small-x data in comparison with the dot-dash lines in Fig. 3(a–d) for Pe = 1, 2, 5, and 10, for parallel-plate ducts. This process was repeated for circular ducts and the results were compared with the dot-dash lines in Fig. 4(a–d). They indicated comparable accuracy similar to those in Fig. 3(a–d) while the deviation due to the curvature effect was relatively small, as expected. Having a correlation for the bulk temperature and Nu_0 from the modified form of Eq. (17a), the value of the asymptotic values of Nu = hH/k_e are computed and they are compared with data appearing in Figs. 5–7(a). The results show good agreements for a relatively large range of the axial coordinate. Also, Figs. 8–10(a) show the behavior of this asymptotic solution for $\mathrm{Nu} = h\, r_0/k_e$, as applied to circular ducts. This indicates that one could use this asymptotic solution in order to determine the heat transfer near the thermal entrance location. The valuable information of this type is attainable with ease without using a series solution that requires a large number of terms.

Furthermore, for flow in porous passages, the condition of a local thermal non-equilibrium exists adjacent to the temperature jump location at the wall. In the formulation of Eq. (17a), the existence of the local thermal equilibrium is commonly hypothesized. However, as x approaches zero, this condition does not exist. There are relations in the literature for estimation of the heat transfer coefficient within the pore. As an example, Wakao and Kaguei [17] presented a correlation for a packed bed of spherical particles as

$$\frac{h}{k_f d} = 2 + 1.1\mathrm{Re}^{0.6}\mathrm{Pr}^{1/3} \tag{23}$$

where $\mathrm{Re} = \varepsilon u_p d/\nu$, and d is the mean diameter of the spherical particles. Also, Minkowycz et al. [18] introduced a relation

$$\frac{hr_h}{k_f} = \frac{0.92}{[1+(A_c - 4\pi r_h^2)/A_c]} \tag{24}$$

where A_c is the mean cross section area of the pores, h is the mean heat transfer coefficient in the pores, and r_h is the pores' hydraulic radius. Moreover, at $x = 0$ location, the wall heat flux is related to $q_w \sim k_e(T_w - T_i)/\varepsilon_p$ where ε_p is the mean pore dimension and this makes

$$\mathrm{Nu}_0 = \frac{h_0 L_c}{k_e} \sim \frac{1}{\varepsilon_p/L_c} \tag{25}$$

Therefore, ax x becomes very small, Nu_0 should remain within the order of this estimated value of L_c/ε_p at $x = 0$ location. Further and detailed studies related to the local thermal non-equilibrium phenomenon in a parallel plate duct are in [19].

5. Conclusion

This study shows that the solutions for heat transfer at small values of x have small dependency on the size of the Peclet number and the functional form of the velocity field described by the Darcy number. As shown in Figs. 3 and 4(a–d), for $x/L_c < 0.05$, the $\mathrm{Nu}_0(x)$ solution has a small dependency on the Darcy number. Also, no flow condition and the slug flow serve as a lower limit and an upper limit.

The approximate values based on asymptotic solution can be useful for estimation of the effects of axial thermal conduction. When the actual information for porous passages is not available, the Nusselt number can be estimated at small x values by interpolation between solutions for clear flow and slug flow for the same Peclet number. Also, one can use information at large and small x values to determine the bulk temperature. Indeed, the determined bulk temperature is useful information in design of the heat transfer devices.

References

[1] W.J. Minkowycz, A. Haji-Sheikh, Heat transfer in parallel-plate and circular porous passages with axial conduction, Int. J. Heat Mass Transfer 49 (13–14) (2006) 2381–2390.
[2] D.A. Nield, A.V. Kuznetsov, M. Xiong, Thermally developing forced convection in a porous medium: parallel plate channel with walls at uniform temperature, with axial conduction and viscous dissipation effects, Int. J. Heat Mass Transfer 46 (4) (2003) 643–651.
[3] A.V. Kuznetsov, M. Xiong, D.A. Nield, Thermally developing forced convection in a porous medium: circular ducts with walls at constant temperature, with longitudinal conduction and viscous dissipation effects, Transport Porous Media 53 (3) (2003) 331–345.
[4] D.A. Nield, A.V. Kuznetsov, Ming Xiong, Thermally developing forced convection in a porous medium: parallel-plate channel or circular tube with isothermal walls, J. Porous Media 7 (1) (2004) 19–27.
[5] A. Haji-Sheikh A., K. Vafai, Analysis of flow and heat transfer in porous media imbedded inside various-shaped ducts, Int. J. Heat Mass Transfer 47 (8–9) (2004) 1889–1905.
[6] A. Haji-Sheikh, W.J. Minkowycz, E.M. Sparrow, Green's function solution of temperature field for flow in porous passages, Int. J. Heat Mass Transfer 47 (22) (2004) 4685–4695.
[7] A. Haji-Sheikh, W.J. Minkowycz, E.M. Sparrow, A numerical study of the heat transfer to fluid flow through circular porous passages, J. Num. Heat Transfer 46 (10) (2004) 929–956.
[8] A. Haji-Sheikh, E.M. Sparrow, W.J. Minkowycz, Heat transfer to flow through porous passages using extended weighted residuals method – a Green's function solution, Int. J. Heat Mass Transfer 48 (7) (2005) 1330–1349.
[9] I. Tiselj, G. Hetsroni, B. Mavko, A. Mosyak, E. Pogrebnyak, Z. Segal, Effect of axial conduction on the heat transfer in micro-channels, Int. J. Heat Mass Transfer 47 (12–13) (2004) 2551–2565.

[10] B. Weigand, D. Lauffer, The extended Graetz problem with piecewise constant wall temperature for pipe and channel flows, Int. J. Heat Mass Transfer 47 (24) (2004) 5303–5312.
[11] M.L. Michelsen, J. Villadsen, The Graetz problem with axial heat conduction, Int. J. Heat Mass Transfer 17 (11) (1974) 1391–1402.
[12] D.A. Nield, A. Bejan, Convection in Porous Media, second ed., Springer-Verlog, New York, 1999.
[13] A. Haji-Sheikh, D.E. Amos, J.V. Beck, Axial heat conduction of heat through a moving fluid in a semi-infinite region, Int. J. Heat Mass Transfer 51 (19–20) (2008) 4651–4658.
[14] A. Haji-Sheikh, J.V. Beck, D.E. Amos, Axial heat conduction effects in the entrance region of parallel plate ducts, Int. J. Heat Mass Transfer 51 (25–26) (2008) 5811–5822.
[15] A. Haji-Sheikh, J.V. Beck, D.E. Amos, Axial heat conduction effects in the entrance region of circular ducts, Heat Mass Transfer 45 (3) (2009) 331–341.
[16] A. Haji-Sheikh, J.V. Beck, Entrance effect on heat transfer to laminar flow through passages, Int. J. Heat Mass Transfer 50 (17–18) (2007) 3340–3350.
[17] N. Wakao, S. Kaguei, Heat and Mass Transfer in Packed Beds, Gordon and Breach Science Publication, 1982.
[18] W.J. Minkowycz, A. Haji-Sheikh, K. Vafai, On departure from local thermal equilibrium in porous media due to a rapidly changing heat source The Sparrow Number, Int. J. Heat Mass Transfer 42 (18) (1999) 3373–3385.
[19] D.A. Nield, A.V. Kuznetsov, M. Xiong, Effect of local thermal non-equilibrium on thermally developing forced convection in a porous medium, Int. J. Heat Mass Transfer 45 (25) (2002) 4949–4955.